Effects of the addition of Nd^{3+} on the structure and magnetic properties of strontium hexaferrites

T. J. Pérez-Juache*
Secretaria de Investigación y Postgrado, UASLP
Dr. Nava S/N, Zona Universitaria. 78290 San Luis Potosí, S. L. P. México

I. Betancourt
Departamento de Materiales Metálicos y Cerámicos
Instituto de investigación en Materiales, Universidad Nacional Autónoma de México
México D.F. 04510, México
Facultad de Ciencias, UASLP
Salvador Nava Martínez, s/n. Zona Universitaria
78290 San Luis Potosí S.L.P., México

S. A. Palomares-Sánchez, M. Mirabal-García
Instituto de Física, Universidad Autónoma de San Luis Potosí
Av. Dr. Nava S/N, Zona Universitaria, 78290
San Luis Potosí, S. L .P. México
(Recibido: 18 de febrero de 2010, Aceptado: 05 de mayo de 2010)

In this work, we present a systematic study on the magnetic properties of Nd^{3+}-susbtituted SrM hexaferrites following the formula $SrNd_xFe_{12-x}O_{19}$, (x = 0.0 - 0.5). The microstructure characterization indicates the formation of a solid solution for Nd contents at x = 0.1, while a composite $Sr(NdFe)_{12}O_{19}/SrFeO_3$ distribution of phases results for x > 0.1. Interesting combination of hard magnetic properties were obtained for the whole compositional series, such as increasing coercivity values of up to 329 kA/m for x = 0.5 with increasing Nd concentration. Results are interpreted in terms intrinsic property variations.

Keywords: Hard magnetic materials; Sr-hexaferrites; Nucleation mechanism

1. Introduction

Magnetic materials with high coercive fields are the basis for fabrication of permanent magnets, which have a very wide range of applications including: loudspeakers, magnetic bearings and couplings, actuators, magnetic catheters, motors (spindle- and stepper- type) and sensors for media storage, consumer electronics, automotive and office automation (VCR´s, camcorders, printers) and in smaller appliances such as watches, clocks, timer switches and cameras and, recently, for "magnetotherapy" [1, 2]. In particular, high coercivity (Sr,Ba)M-type hexagonal ferrites, which were developed during the 1950´s [3], have received considerable attention in order to improve their magnetic capabilities because of their low price per unit of stored energy, which allows competitive large scale production, together with their excellent chemical stability and high Curie temperature. For instance, many studies have focused on cationic substitutions and on ionic radius considerations, such as light rare-earth ions like La or Pr replacing (Sr,Ba) [4, 5] or Nd, La, Co replacing (Fe) in (Sr, Ba)-hexaferrites[6, 7, 8]. Replacement of divalent Ba or Sr by trivalent La has been reported as causing a valence change of one Fe^{3+} per formula unit into Fe^{2+} [9], whereas the substitution of Fe^{3+} by Nd^{3+} preserves the charge distribution within the unit cell. In earlier works it was reported that the substitution of Fe^{3+} by Nd^{3+} in BaM-type enhanced the material´s coercivity showing a maximum value of 437 kA/m as a consequence of the reduced particle size observed for such hexagonal $BaNd_xFe_{12-x}O_{19}$ powders synthesized by high-temperature sol-gel auto-combustion method [6]. On the other hand, Nd^{3+} additions into SrM-type hexaferrites, according to the formula $Sr_{1-x}Nd_xFe_{12}O_{19}$, were reported as having a beneficial effect on the material´s coercivity without causing a significant deterioration neither on the saturation magnetization nor on the remanence [10, 11]. In this work, we prepared the M-type hexaferrites series $SrNd_xFe_{12-x}O_{19}$ (x= 0.0 – 0.5) by means of the ceramic method in order to determine their crystalline structure, phase distribution and magnetic properties.

2. Experimental details

The hexaferrite series $Sr_{1-x}Nd_xFe_{12}O_{19}$ (x = 0.0-0.5) were prepared by using the conventional ceramic process. Initially, a mixture of α-Fe_2O_3, $SrCO_3$ and Nd_2O_3 powders (in stoichiometric proportion) was weighted and mixed for 2 h at 90 rpm in a planetary ball milling unit, followed by calcination in air at 900°C for 1 h. The fired powders were

*tere.p.juache@hotmail.com

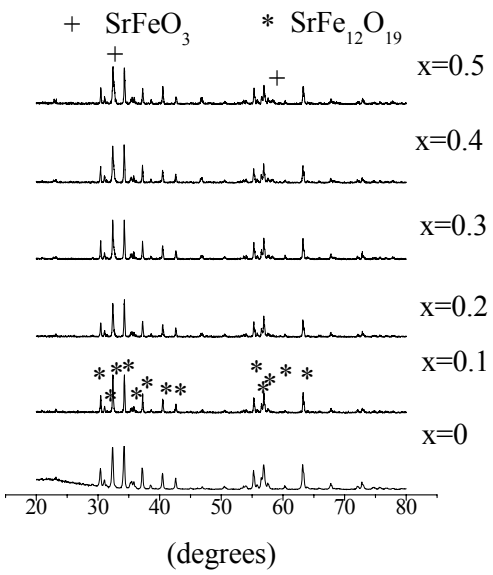

Figure 1. XRD patterns for the hexaferrite $SrNd_xFe_{12-x}O_{19}$ series.

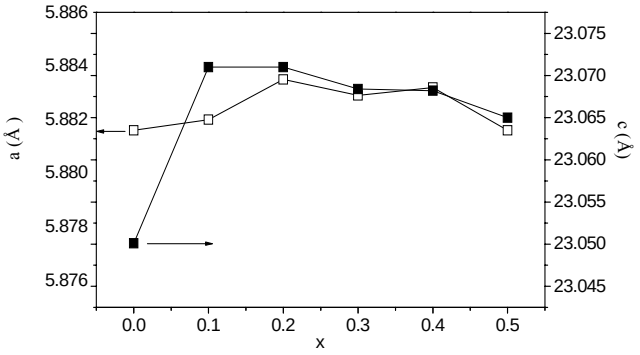

Figure 2. Unit cell parameters ***a*** and ***c*** as a function of Nd content for hexaferrite $SrNd_xFe_{12-x}O_{19}$ series.

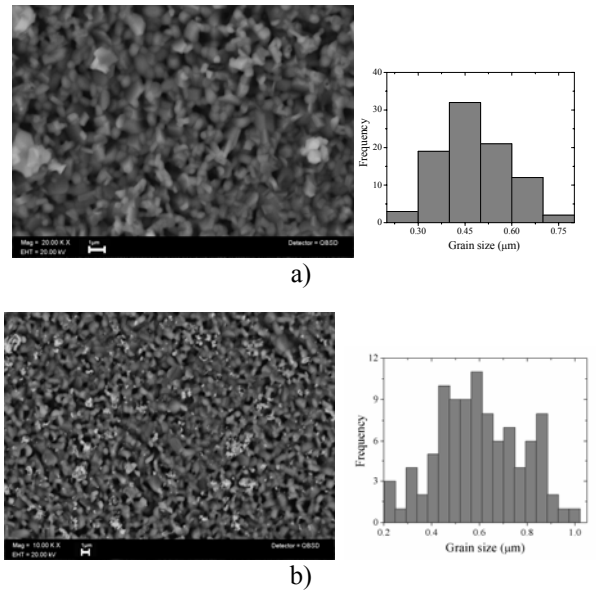

Figure 3. SEM micrographs for (a) SrM and (b) $SrNd_{0.4}Fe_{11.6}O_{19}$ hexaferrite samples.

then pressed into pellets with polyvinyl alcohol (PVA) acting as a binder, for a subsequent sinterization process at 1200°C for 1 h in air. Phase distribution and unit cell variation were determined by means of powder X-ray diffraction (XRD) analysis in a Bruker AXS D8 equipment together with Rietveld [12] analysis performed with the open-access MAUD program [13]. Scanning Electron Microscopy (SEM) observations in a Leica Stereoscan 440 at 20 kV afforded verification of grain morphology and their mean size. On the other hand, the magnetic properties at room temperature (maximum magnetization $\mu_0 M_{max}$, remanence magnetization $\mu_0 M_r$, intrinsic coercivity H_c and maximum energy product $(BH)_{max}$) were determined by means of Vibrating Sample Magnetometry with a LDJ9600 equipment at a maximum applied field of 1200 kA/m.

3. Results and discussion

3.1Crystal structure investigation and phase distribution analysis

The X-ray diffraction patterns for the whole compositional series $SrNd_xFe_{12-x}O_{19}$ are shown in Figure 1. For all the diffractograms, the main peaks at 2θ = 1.904,2.079,1.938, 2.007, 1.854, 2.019, 1.872, 1.901, 1.923, 1.886,1.868, 1.982, corresponding to the (110), (008), (114), (107), (201), (108), (203), (205), (217), (306), (304), (2011), (220) diffraction planes, respectively, can be associated with the hexagonal M-type phase. For x = 0.0 and 0.1 compositions, no extra peaks related to secondary phases are observed, reflecting the formation of a solid solution for these Nd concentration. In contrast, for increasing Nd content x, some additional peaks corresponding to the $SrFeO_3$ phase appear with enhancing intensities for higher x concentrations. According to Rietveld analysis, this secondary phase increases its volume fraction with increasing x content up to a maximum of 13.5 % for x = 0.5. The increasing presence of this $SrFeO_3$ phase is due to the increasing excess of Nd_2O_3 used during the synthesis process [14]. A resume of phase distribution is shown in Table 1. On the other hand, the unit cell parameters a and c as a function of Nd content is displayed in Figure 2, for which a shallow dependence with x is manifested, which suggests the Nd incorporation into the crystal SrM structure.The initial increments observed for both a, c parameters can be ascribed to the considerable larger ionic radii of Nd^{3+} (0.98 Å) compared with Fe^{3+} (0.65 Å for octahedral sites and 0.49 Å for tetrahedral sites) [15].

3.2 Microestructal characterization

SEM micrographs corresponding to $SrFe_{12}O_{19}$ and $SrNd_{0.4}Fe_{11.6}O_{19}$ hexaferrite samples are shown in Figure 3. For the initial SrM sample (Figure 3a), an isotropic distribution of polyhedral grains with average size of

Table 1. Phase distribution and their relative proportion (%) for the hexaferrite $SrNd_xFe_{12-x}O_{19}$ series according to Rietveld analysis.

x	Phase	Proportion (%)
0	$SrFe_{12}O_{19}$	($SrFe_{12}O_{19}$) 100%
0.1	$SrNd_{0.1}Fe_{11.9}°_{19}$	($SrNd_{0.1}Fe_{11.9}°_{19}$) 100%
0.2	$SrNd_{0.2}Fe_{11.8}°_{19}$	95.16%
	$SrFeO_3$	4.83%
0.3	$SrNd_{0.3}Fe_{11.7}O_{19}$	92.35%
	$SrFeO_3$	7.71%
0.4	$SrNd_{0.4}Fe_{11.6}O_{19}$	89.57%
	$SrFeO_3$	10.42%
0.5	$SrNd_{0.5}Fe_{11.5}O_{19}$	86.46%
	$SrFeO_3$	13.53%

0.45μm is evident. In addition, the back-scattered electron contrast is consistent with a single phase grain distribution. On the other hand, for the x=0.4 sample (Figure 3b), a similar polycrystalline microstructure is observed but with a mean size of 0.6 μm, besides the presence of numerous minute grains (< 0.25 μm) of different composition, relative to the main constituent grains.

3.3. Magnetic properties

Figure 4 illustrates the hysteresis *M-H* curve for the original $SrFe_{12}O_{19}$ hexaferrite sample, which displays characteristic hard magnetic properties, i.e, a large coercivity value of 257 kA/m, together with good remanence $\mu_0 M_r$ = 0.25 T and maximum energy product $(BH)_{max}$ = 11 kJ/m^3. Since the magnetization *M* did not reach the saturation state, the maximum magnetization $\mu_0 M_{max}$ value is used in the following data analysis.

Room temperature magnetic properties as function of Nd content for the whole hexaferrite $SrNd_xFe_{12-x}O_{19}$ series are shown in Figure 5. Both $\mu_0 M_{max}$ and $\mu_0 M_r$ (Figure 5a) seems to have a maximum at x =0.1 followed by a decreasing tendency. The maximum in magnetization might be related to the initial expansion of the unit cell (Fig.2) since such kind of crystal cell enlargement favours the cooperative orientation of the magnetic moments and thus, the increase of magnetization [16], with the $(BH)_{max}$ product (Figure 5b) having a similar behaviour. On the other hand, H_c exhibits a monotonous increase from 259 kA/m to 329 kA/m with increasing x concentration (Figure 5c).

The marked reduction of $\mu_0 M_{max}$ and $\mu_0 M_r$ beyond x = 0.1 is a consequence of the increasing precipitation of the secondary paramagnetic SrFe-containing phase, which

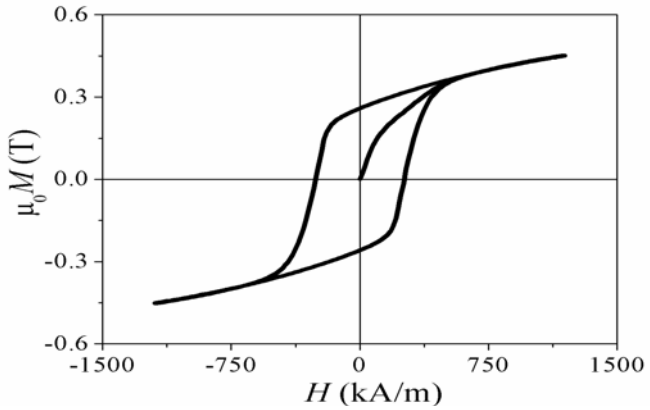

Figure 4. Figure 4. Hysteresis *M-H* curve for the $SrFe_{12}O_{19}$ hexaferrite.

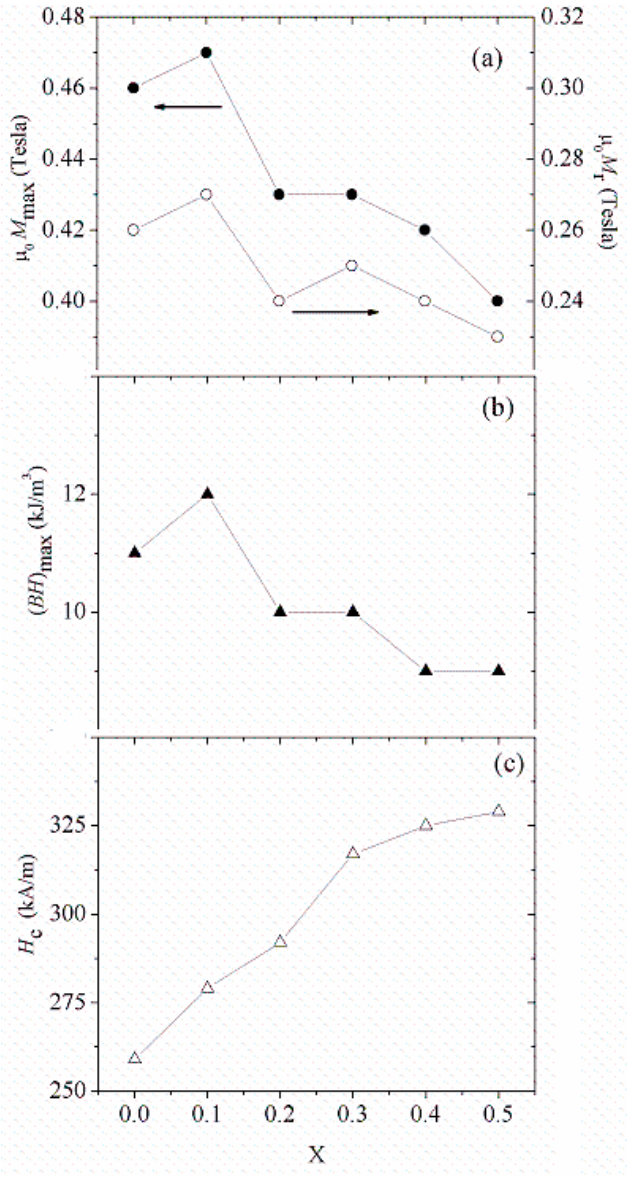

Figure 5. Magnetic properties for the hexaferrite $SrNd_xFe_{12-x}O_{19}$ series (solid lines are only a guide for the eye).

causes a dilution effect of $\mu_0 M_{max}$. Complementary, the tendency observed for the $(BH)_{max}$ with the Nd content follows the $\mu_0 M_r$ behavior since the condition $\mu_0 H_c > 0.5\mu_0 M_r$ is fulfilled, which also enables the possibility of maximum $(BH)_{max}$ for anisotropic materials [17]. On the other hand, the progressive coercivity enhancement with increasing Nd content can be analyzed within the frame of the nucleation-controlled coercivity mechanism of coupled grains [17], for which, on first approximation, the coercivity H_c of polyhedral particles is proportional to the nucleation field H_N and to the saturation magnetization $\mu_0 M_s$ according to

$$H_C = H_N - N_{eff} M_s \quad (1)$$

where N_{eff} stands for an effective demagnetizing factor caused by stray fields at sharp corners and edges of polyhedral grains. H_N represents the field intensity necessary for nucleation of a reversed domain after the saturation, and is given by:

$$H_N = \frac{2K_1}{\mu_0 M_s} \quad (2)$$

with K_1 as the magnetocrystalline anisotropy constant. Assuming that the tendency observed for $\mu_0 M_{max}$ in Figure 5 is a representative approximation for $\mu_0 M_s$ as a function of x, it is possible to explain the improving H_c observed across the Nd variation on the basis of an enhancing effect on the nucleation field H_N as a consequence of the rapid decrease of μM_s values with x (Figure 5).

4. Conclusion

The magnetic properties for the M-type hexaferrite $SrNd_xFe_{12-x}O_{19}$ series, obtained by conventional ceramic method, showed a strong dependence with Nd content, with interesting combination of H_c = 329 kA/m, $(BH)_{max}$ = 5 kJ/m^3 and $\mu_0 M_{max}$ = 0.35 T for x = 0.5 . Maximum substitution rate for the formation of (Sr,Nd)M solid solution was observed at x = 0.1.

Acknowledgment

T. J. Perez-Juache is grateful for the scholarship granted by Conacyt-México and by the student mobility program ECOES, México, as well as for the valuable technical support given by G. Gabriel López R during materials processing and characterization.

References

[1]. I. Betancourt, Rev. Mex. Fis. **48**, 283 (2002).
[2]. E. du Tremolet de Lacheisserie and P.R. Ochette in Magnetism. Materials and Applications. Ed. E. du Tremolet de Lacheisserie, Springer, New York, 433-439 (2003).
[3]. H. Kojima, in E.P. Wohlfarth (Ed), Ferromagnetic Materials, North-Holland, Amsterdam, **3**, 305(1982).
[4]. M. Küpferling, P. Novák, K. Dnízek, M.W. Pieper, R. Grössinger, G. Wiesinger M. Reissner, J. Appl. Phys. **97**, 10F309 (2005).
[5]. Wang, C.B. Ponton, I.R. Harris, J. Alloys Compd., **403,** 104(2005).
[6]. G. Rui-quian, LI Hong-gui, S. Pei-mei, L. Yun- jiao, Z. Zhong-wei, L. Mao-sheng, J. Cent. South Univ. Technol, **82**, 130(2001).
[7]. C. Doroftei, E. Rezlescu, P.D. Popa, N. Rezlescu, Journal of Optoelectronics and Advanced Materials, **8**, 1023(2006).
[8]. Kajal K. Mallick, Philip Shepherd, Roger J. Green, J. Magn. Magn. Mater. **312**, 418 (2007).
[9]. X.Liu, W. Zhong, S. Yang, Z. Yu, B. Gu, y. Du, J. Magn. Magn. Mater. **238,** 207 (2002).
[10]. J. F. Wang, C.B. Ponton, and I.R. Harris, IEEE Trans. Magn. Magn., **38**, 2928 (2002).
[11]. S. Bindra and I. Hudiara, Journal of Ceramic Processing Research, **7**, 113 (2006).
[12]. G. Will. Powder Diffraction. Ed. Springer, 41(2006).
[13]. M. Ferrari, L. Lutterotti, J. Appl. Phys., **76,** 7246 (1994).
[14]. P. Sharma, A. Verma, R.Sidhu, O. Pandey, J. Alloys Compd, **361**, 257 (2003).
[15]. R. Valenzuela, Magnetic Ceramics, Ed. Cambridge University Press. (Cambridge, 1994).
[16]. B.D. Cullity, C.D. Graham, Introduction to Magnetic Materials, 2nd ed, J.Wiley & ons, Hoboken N.J., (2009).
[17]. H. Kronmuller, F. Manfred, Micromagnetism and Microstructure of Ferromagnetic Solids. Cambridge University Presss, (Cambridge 2003).